

Stochastic Regimes in the Driven Oscillator with a Step-Like Nonlinearity

S. V. Bulanov,¹ A. Yogo,² T. Zh. Esirkepov,¹ J. K. Koga,¹ S. S. Bulanov,³ K. Kondo,¹ and M. Kando¹

¹*Japan Atomic Energy Agency, Kansai Photon Science Institute,
8-1-7 Umemidai, Kizugawa-shi, Kyoto, 619-0215 Japan*

²*Institute of Laser Engineering, Osaka University, Suita 565-0871, Osaka, Japan*

³*Lawrence Berkeley National Laboratory, Berkeley, California 94720, USA*

(Dated: September 14, 2021)

A nonlinear oscillator with an abruptly inhomogeneous restoring force driven by an uniform oscillating force exhibits stochastic properties under specific resonance conditions. This behaviour elucidates the elementary mechanism of the electron energization in the strong electromagnetic wave interaction with thin targets.

1. INTRODUCTION

Chaos in nonlinear dynamics plays a fundamental role in understanding the properties of various physical systems [1]. A driven Duffing oscillator is an important example which demonstrates chaotic behaviour [2]. In particular, the problem of revealing the conditions for realization of chaotic regimes is of high importance for developing the theoretical description of strong electromagnetic wave interaction with matter. This is connected to the mechanisms of charged particle energization in collisionless plasmas (this is also called ‘anomalous heating’), in their interaction with high intensity electromagnetic waves. As an example we note here the well known electron ‘vacuum heating’ by laser radiation which occurs at the plasma-vacuum interface [3]. Such processes have been invoked as an elementary mechanism of collisionless absorption of electromagnetic waves and of electron heating during high power laser interaction with various targets (e.g. see [4]). Revealing of the elementary electron heating mechanism is important for developing laser plasma sources of both fast electrons and ions.

Among the ion acceleration mechanisms target normal sheath acceleration (TNSA) [5] has been the most intensively investigated. The TNSA mechanism crucially depends on the plasma electron heating. It implies that the accelerated ion energy is proportional to the mean electron energy. The anomalous heating of electrons at the plasma-vacuum interface has been noted in Refs. [6, 7], where it was found that due to stochastic heating the energy of the electrons recirculating around a small size target can be substantially higher than the energy of the electron quivering in the field of the electromagnetic wave. Taguchi et al., [6] in analysing the results of the particle-in-cell simulations have called this regime ‘non-linear resonance absorption’. Finding the conditions and criteria of the realization of such a regime can have important consequences, in particular, for optimizing the laser-target parameters in developing a laser ion accelerator. Stochastic regimes in the electromagnetic wave interaction with a thin foil target have been found in theoretical papers [8, 9]. We note here also the electron

heating by a strong electromagnetic field due to the electron rescattering off ions [10–12].

Below we analyze a model of a driven oscillator with a step-like nonlinearity in order to determine and elucidate the conditions when the stochastic vacuum heating takes place. The 3-dimensional model used bears the key features of the problem addressed in Refs. [8, 9, 13, 14], but in a significantly simpler mathematical approximation, because a full description of the charged particle interaction with electromagnetic waves implies a consideration of a 7-dimensional dynamical system. In addition, such a mathematically simple system can lead to a broader understanding of the underlying physical processes of electromagnetic field interaction with charged particles, thus leading to developing novel theoretical tools.

The paper is organized as it follows. In Section 2 we formulate the mathematical model of the nonlinear driven oscillator and analyze the properties of its free and driven oscillations. We obtain the discrete mapping and find the threshold of stochastic regimes. The trajectory diffusion is described by the Kolmogorov-Fokker-Planck equation (KFPE) whose analytical solution is presented. Using the KFPE solution we derive the asymptotic dependence on time of the average electron momentum. Then, in Section 3, we present the result of the numerical integration of the equations describing the trajectories of the driven oscillator with a step-like nonlinearity in nonrelativistic and relativistic limits, in regular and stochastic regimes. Here the time averaged electron kinetic energy is found numerically. At the end of the paper, in the Conclusion, we summarize the obtained results.

2. DRIVEN OSCILLATOR WITH A STEP-LIKE NONLINEARITY

We consider the system of ordinary differential equations

$$\dot{p} + \varepsilon_p \text{sign}(x) = a \cos t, \quad (1)$$

$$\dot{x} = \frac{p}{(1 + p^2)^{1/2}}. \quad (2)$$

Here the sign function $\text{sign}(x) = 1$ for $x > 0$ and $\text{sign}(x) = -1$ for $x < 0$, and the dots denote differentiation with respect to time, t . The driver force on the r. h. s. of Eq. (1) represents the electromagnetic wave within the framework of the dipole approximation.

In the case of the electron circulating around a thin foil target, p and x are the electron momentum and coordinate normalized by $m_e c$ and c/ω , respectively, where m_e is the electron mass, ω is the driver field frequency, c is the light speed in vacuum. In Eqs. (1, 2) the time variable is normalized by ω^{-1} . The parameter

$$\varepsilon_p = \frac{2\pi n_0 e^2 l_0}{m_e \omega c}, \quad (3)$$

introduced in Ref. [15], is proportional to the charge separation electric field, $E_{cs} = 2\pi e n_0 l_0$, normalized by $m_e \omega c/e$, for a thin foil with the charge surface density equal to $e n_0 l_0$. The driver field normalized amplitude on the r. h. s. of Eq. (1) equals

$$a = \frac{e E_0}{m_e \omega c}. \quad (4)$$

If the driver field vanishes, $a = 0$, the system of equations (1, 2) describes free oscillations of a relativistic oscillator with an abruptly changing restoring force. The energy integral of Eqs. (1, 2) is given by

$$(1 + p^2)^{1/2} + \varepsilon_p |x| = \mathcal{E}. \quad (5)$$

Using this integral, we find the momentum and coordinate dependence in time for the case of free oscillations:

$$p = p_m + \text{sign}(x) \varepsilon_p t, \quad (6)$$

$$x = x_0 + \text{sign}(x) \frac{\mathcal{E} - [1 + (p_m - \varepsilon_p t)^2]^{1/2}}{\varepsilon_p}, \quad (7)$$

with the constant \mathcal{E} on the r. h. s. of Eq. (7) equal to

$$\mathcal{E} = [1 + (p_m - \varepsilon_p t)^2]^{1/2} + \varepsilon_p |x_0|. \quad (8)$$

It is determined by the initial values of the momentum p_m and coordinate x_0 .

Using relationships (6) and (7) we find the period of nonlinear oscillations

$$T = \frac{4p_m}{\varepsilon_p} \quad (9)$$

depending on their amplitude p_m .

Now we consider the case of driven oscillations, when $a \neq 0$, i.e. the electron moves in the superposition of the the static inhomogeneous electric field, $-\varepsilon_p \text{sign}(x)$, and oscillating homogeneous field, $a \cos t$. This is described by the system of equations (1,2) with the Hamiltonian

$$\mathcal{H}(x, p, t) = (1 + p^2)^{1/2} + \varepsilon_p |x| - a x \cos t. \quad (10)$$

The solution of Eqs. (1,2) can be written in terms of piecewise-smooth functions. Let the initial condition at $t = t_0$ be $x(t_0) = x_0$, and $p(t_0) = p_0$. Let t_k be consecutive zeros of the function $x(t)$, $k = 1, 2, 3, \dots$ (it is possible that $t_1 = t_0$, but not required).

The solution to $p(t)$ in the interval $t \in [t_n, t_{n+1}]$ is

$$p(t) = p_0 + \varepsilon_p S_0 \left(2 \sum_{k=1}^n (-1)^k t_k + t_0 + (-1)^{n+1} t \right) + a(\sin t - \sin t_0) \quad (11)$$

where

$$S_0 = \begin{cases} \text{sign}(x_0), & x_0 \neq 0, \\ \text{sign}(p_0), & x_0 = 0, p_0 \neq 0, \\ \text{sign}(\cos(t_0)), & x_0 = p_0 = 0, \cos(t_0) \neq 0, \\ -\text{sign}(\sin(t_0)), & x_0 = p_0 = \cos(t_0) = 0. \end{cases} \quad (12)$$

Then for $x(t)$ we have

$$x(t) = \int_{t_0}^t \frac{p(t)}{(1 + p(t)^2)^{1/2}} dt. \quad (13)$$

The consecutive zeros of the function $x(t)$ are determined by the implicit relationships

$$\int_{t_k}^{t_{k+1}} \frac{p(t)}{(1 + p(t)^2)^{1/2}} dt = 0, \quad k = 0, 1, 2, \dots \quad (14)$$

Loops are possible, if there exist integers $n \geq 2$ and $m \geq 1$, such that the momentum at t_n is the same as at t_1 , $p_n - p_1 = 0$, and the phase of the oscillating component of the force is the same, $t_n - t_1 = 2\pi m$. This leads to the condition

$$2 \sum_{k=2}^n (-1)^k t_k - t_1 + (-1)^{n+1} t_n = 0, \quad t_n = t_1 + 2\pi m. \quad (15)$$

While the electron trajectory crosses the $x = 0$ plane, the sign of the static electric field changes abruptly. This can be considered as a ‘‘collision’’, during which the oscillating driver electric field produces work changing the electron energy. Depending on the phase, when the ‘‘collision’’ happens, the work can be either positive or negative, resulting in the electron energy increasing or decreasing.

A characteristic electron momentum change during the $x = 0$ plane crossing can be estimated to be of the order of

$$\Delta p = a. \quad (16)$$

The enhancement of the energy transfer from the driver electric field to the electron is expected to occur when a resonant like condition takes place, i. e. when the

periods of the motion of the electron in subsequent periods of the free oscillations with momenta p and $p + \Delta p$ are co-measurable with the period of the driver electric field, 2π . This yields

$$\frac{p}{\varepsilon_p} = \frac{\pi}{2} j \quad (17)$$

and

$$\frac{p + \Delta p}{\varepsilon_p} = \frac{\pi}{2} k \quad (18)$$

with $j = 1, 2, 3, \dots$ and $k = 2, 3, 4, \dots$. From these expressions it follows that the resonance condition is

$$a = \frac{\pi(k-j)}{2} \varepsilon_p. \quad (19)$$

This gives a relationship between the parameter ε_p and the normalized driver amplitude, a , which can be rewritten in terms of the static and oscillating electric fields as $E_{cs} \approx E_0$. Here and further it is assumed that $k - j = 1$. We note here that the condition (19) is equivalent to the criterion of thin slab relativistic transparency [15–18] as well as determining the optimal parameters for ion acceleration by the laser light radiation pressure [17–20].

Using Eqs. (16–19) we can find the electron momentum time dependence in the regimes of regular and stochastic acceleration.

In the regular acceleration regime, the electron energy increases with $\Delta p = a$ during each half-period of free oscillations. Taking into account the free oscillation period dependence on the electron momentum (9) we obtain that the maximum of the momentum grows in proportion to the square root of time,

$$p_m = (a\varepsilon_p t/2)^{1/2} = a(t/\pi)^{1/2}. \quad (20)$$

In order to describe the stochastic acceleration let us assume that the trajectory crosses the $x = 0$ plane at the instants of time equal to t_n . The momentum change is

$$p_{n+1/2} = p_n - \varepsilon_p(t_{n+1/2} - t_n) + a \sin(t_n), \quad (21)$$

$$p_{n+1} = p_{n+1/2} + \varepsilon_p(t_{n+1} - t_{n+1/2}) + a \sin(t_{n+1/2}). \quad (22)$$

In the limit of large momentum

$$|p_n|/a\varepsilon_p \gg 1 \quad (23)$$

the time interval between two subsequent crossings of the $x = 0$ plane is equal to

$$t_{n+1} - t_n = \frac{4|p_{n+1}|}{\varepsilon_p}. \quad (24)$$

Here we have neglected the contribution of the order of a . Introducing the phase $\phi_n = t_n$ we rewrite expressions (21–24) in the form of the Poncaré map:

$$p_{n+1} = p_n + 2a \sin(\phi_n), \quad (25)$$

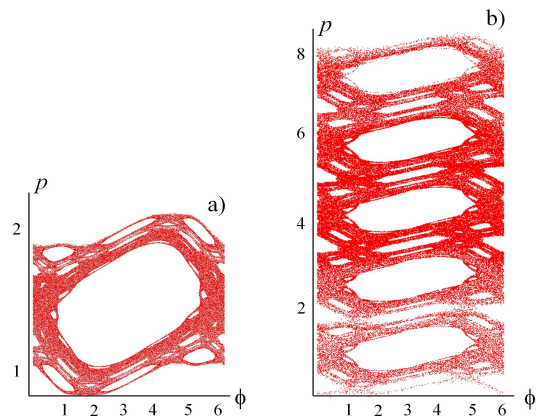


FIG. 1. Phase portrait (ϕ, p) of the mapping (25,26) for $\varepsilon_p = 1$, $p_0 = 1$ and $\phi_0 = \pi/3$. a) The stochastic layer formation for $a = 0.25$. b) The stochastic sea $a = 0.3$.

$$\phi_{n+1} = \phi_n + \frac{4|p_{n+1}|}{\varepsilon_p} \pmod{2\pi}, \quad (26)$$

which is also known as the standard map, corresponding to the model describing stochastic Fermi acceleration [21, 22] as a material point bouncing between two oscillating walls, e. g. see [23, 24]. As is well known a Jacobian of the mapping is equal to unity,

$$\frac{(\partial p_{n+1}, \partial \phi_{n+1})}{(\partial p_n, \partial \phi_n)} = 1, \quad (27)$$

i.e. the mapping conserves the phase volume. Due to the condition of the driver amplitude smallness (23) the momentum change during subsequent crossing of the $x = 0$ plane is relatively small while the phase ϕ can change significantly. Using this fact we can obtain from Eqs. (25) and (26) that

$$\phi_{n+1} \approx \phi_n + \frac{4|p_n|}{\varepsilon_p} + \frac{8|p_n|a}{\varepsilon_p} \sin(\phi_n). \quad (28)$$

This expression yields for the phase volume stretching along the ϕ coordinate

$$|K| \approx \left| \frac{\delta \phi_{n+1}}{\delta \phi_n} - 1 \right| \approx \frac{8a|p_n|}{\varepsilon_p} \cos(\phi_n). \quad (29)$$

Since in the case of "highest probability" $|\cos(\phi_n)| \approx 1$, the criterion of the stochastic regime onset is $|K| > 1$ or

$$\frac{8a|p_n|}{\varepsilon_p} > 1. \quad (30)$$

In Fig. 1 we show the phase portraits (ϕ, p) of the mapping (25,26) at the stochasticity threshold (a), and in the stochastic regime (b), when the particle energy can grow.

Eq. (25) yields for the averaged squared deviation of the momentum change during one cycle

$$\overline{(\Delta p)^2} = \overline{(p_{n+1} - p_n)^2} = \overline{4a^2 \sin^2(\phi_n)} = 2a^2. \quad (31)$$

According to Eq. (9) the cycle duration is equal to $\tau = 4|p|/\varepsilon_p$. This gives

$$\overline{(\Delta p)^2} = \frac{a^2 \varepsilon_p \tau}{2|p|}, \quad (32)$$

which shows that the momentum dependence on time has a character of diffusion with the diffusion coefficient

$$D_{pp} = \frac{\Delta p \Delta p}{\tau} = \frac{a^2 \varepsilon_p}{2|p|}. \quad (33)$$

Introducing the distribution function $f(t, p)$, which obeys the KFPE, we write this equation as

$$\partial_t f = \frac{1}{2} \partial_p (D_{pp} \partial_p f), \quad (34)$$

or

$$\partial_t f = \frac{a^2 \varepsilon_p}{4} \partial_p \left(\frac{1}{|p|} \partial_p f \right). \quad (35)$$

The solution of the KFPE for the initial condition $f(t=0, p) = n_0 \delta(p)$, where $\delta(p)$ is the Dirac delta function, can be easily found. It reads

$$f = n_0 \frac{3^{1/3}}{(8\kappa t)^{1/3} \Gamma(1/3)} \exp\left(-\frac{|p|^3}{9\kappa t}\right) \quad (36)$$

where

$$\kappa = \frac{a^2 \varepsilon_p}{2} \quad (37)$$

and $\Gamma(x)$ is the Euler gamma function [25].

Using Eq. (36) we can find the time dependence of the average electron momentum,

$$\bar{p} = \int p f(p) dp. \quad (38)$$

It is given by

$$\bar{p} = \frac{3^{2/3} \Gamma(2/3)}{2\Gamma(1/3)} (\kappa t)^{1/3} = \frac{3^{2/3} \Gamma(2/3)}{2^{4/3} \Gamma(1/3)} (a^2 \varepsilon_p t)^{1/3}. \quad (39)$$

with the momentum dependence on time $p \sim t^{1/3}$.

The average kinetic energy,

$$\frac{\overline{\mathcal{E}_e}}{m_e c^2} = \int_{-\infty}^{+\infty} [(1+p^2)^{1/2} - 1] f(p) dp \quad (40)$$

can be written in terms of the Meijer G - function [25]

$$\frac{\overline{\mathcal{E}_e}}{m_e c^2} = - \left[1 + \frac{G_{3,5}^{5,3} \left(\frac{1}{324(\kappa t)^2} \left| \begin{array}{c} 1/6, 1/2, 5/6 \\ -1/3, 0, 0, 1/3, 1/2 \end{array} \right. \right)}{48 \times 3^{1/6} \pi^3 (\kappa t)^{1/3}} \right]. \quad (41)$$

In the limit of small but finite momentum this expression yields

$$\frac{\overline{\mathcal{E}_e}}{m_e c^2} \approx \frac{\Gamma(1/3)\Gamma(1/6)\Gamma(5/6)}{4\pi^2} (\kappa t)^{2/3} = 1.6151 (\kappa t)^{2/3}. \quad (42)$$

When $t \rightarrow \infty$ we have

$$\frac{\overline{\mathcal{E}_e}}{m_e c^2} \approx \frac{2^{2/3} \pi^{3/2} \Gamma(1/6)}{3^{4/3} \Gamma(1/3)^2 \Gamma(2/3)^2} (\kappa t)^{1/3} = 1.051 (\kappa t)^{1/3}. \quad (43)$$

The energy dependence on time, $\overline{\mathcal{E}_e} \sim t^{1/3}$, has been noted in Ref. [8].

The above derived standard map given by Eqs. (25,26), the KFPE equation (35), and the KFPE solution (36), showing the estimations for the stochasticity threshold (30) and the heating rate (39), have been obtained by using certain assumptions, which correspond to the conditions imposed by Eqs. (16, 23, 28). Since, as is well known, the properties and behaviour of dynamical systems in the stochastic regimes are very sensitive to the parameters, below we present the results of numerical integration of the equations of motion in classical and relativistic limits. They provide additional information on the properties of a driven oscillator with a step-like nonlinearity.

3. RESULTS OF NUMERICAL SOLUTIONS OF THE EQUATIONS DESCRIBING DRIVEN OSCILLATIONS

In order to analyse in more detail the chaotic v.s. regular dynamics of the driven nonlinear oscillator we have integrated Eqs. (1, 2) numerically for different parameters. In order to regularize the singularity on the left hand side of Eq. (1) we use instead of $\text{sign}(x)$ the function $\text{Tanh}(x/l)$ with the width l substantially smaller than the typical particle displacement. In dimensional variables this requires $l \ll eE/m_e \omega_{pe}^2$, where $\omega_{pe} = (4\pi n e^2/m_e)^{1/2}$ is the Langmuir frequency.

The oscillator dynamics exhibits principally different behaviour depending on the relative values of the parameter ε_p and driver amplitude a . When the normalized driver amplitude is substantially less than unity, $a \ll 1$, we have the non-relativistic limit with nonlinear effects due to the abrupt dependence of the restoring force on the coordinate. In opposite limit, when $a \gg 1$, in addition there is a nonlinearity due to the relativistic relationship between the velocity and momentum (2).

Non-relativistic regime

In the classical limit the behaviour of the driven nonlinear oscillations is determined by one dimensionless pa-

parameter, $b = a/\varepsilon_p$, which can be written as

$$b = \frac{E_0}{2\pi enl}. \quad (44)$$

This is equal to the ratio of the driver electric field to the electric field formed by a thin foil with the electric charge surface density $2\pi enl$. The system of equations (1) and (2) takes the form

$$\ddot{x} + \text{sign}(x) = b \cos(t). \quad (45)$$

Here the x variable is normalized by $c/\omega\varepsilon_p = m_e c^2/2\pi e^2 nl = d_e^2/l$ with $d_e = c/\omega_{pe}$ being the collisionless skin depth. We shall also use the notation $p = \dot{x}$.

In the case of free oscillations when the r. h. s. of Eq. (45) vanishes, i. e. $b = 0$, the energy integral (5) takes the form

$$\frac{p^2}{2} + |x| = \mathcal{E} \quad (46)$$

with the constant $\mathcal{E} = p_0^2/2 + |x_0|$. The period of free oscillations is given by Eq. (9), which in the notations used in this subsection is $T = 4p_m$.

The resonance condition (19) in the non-relativistic limit yields

$$b = \pi/2. \quad (47)$$

If the driver amplitude is substantially smaller than unity, for the initial conditions $p_0 = 0$ and $x_0 = 0$ the trajectory is confined in the vicinity of the equilibrium $x = 0$ within the region $|x| \ll l$.

For the driver amplitude approaching the threshold (47) the oscillations become nonlinear with the excursion exceeding the width l as seen in the case shown in Fig. 2 when the chosen parameters are close, but below the threshold (47). The dependence of the momentum and coordinate on time in Figs. 2 (a) and (c) correspond to nonlinear oscillations with slowly varying period and amplitude. In the phase plane, Fig. 2 (b), it is seen that the trajectory is confined within finite domain. In Fig. 2 (d) we plot the Poincaré section showing the particle positions in the phase plane (x, p) at the discrete time with the time step equal to the period of the driving force, 2π . The loop trajectory is slightly broadened due to approaching the stochastic regime.

There is a difference between the Poincaré sections presented here, and below in Figs. 3 (d), 4 (b,d,f), 5 (d), 6 (d), 8 (a), 11 (b), and in 12 (b), and those Poincaré sections which are shown in Figs. 1 (a) and (b). The driven oscillator dynamics is characterized by two time scales: the period of the driver force and the time interval between subsequent crossing by the trajectory the plane at $x = 0$. While in Fig. 1 and in Fig. 8 (b) each point in the plane (ϕ, p) corresponds to the particle momentum and the phase calculated for the time when the

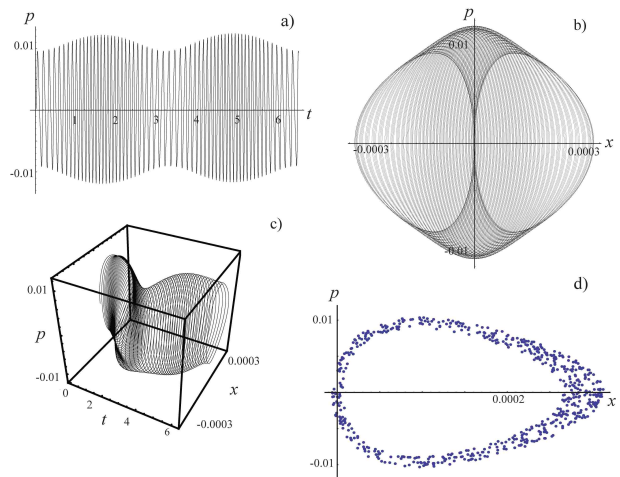


FIG. 2. Driven oscillations below the stochastic regime in the case of $b = 0.775$, $l = 0.000125$, $p_0 = 0$, and $x_0 = 0$. a) The momentum p v.s. time. b) The phase plane (x, p) for $t \in [0, 10 \times 2\pi]$. c) The configuration space (t, x, p) for $t \in [0, 10 \times 2\pi]$. d) The Poincaré section showing the particle positions in the phase plane (x, p) at the discrete time with the time step equal to the period of the driving force, 2π .

trajectory crosses of the plane at $x = 0$, the points in the phase planes (x, p) presented in Figs. 3 (d), 4 (b,d,f), 5 (d), 6 (d), 11 (b), and in 12 (b) show the particle coordinate and momentum at the subsequent instants of time separated by the driver force period.

For the driver amplitude slightly above the stochasticity threshold being equal to $b = 0.795$ the oscillations become apparently stochastic as clearly seen in Fig. 3. During the initial interval of time $t \in [0, 50]$ the oscillations have a relatively low, gradually growing amplitude as seen in Figs. 3 (a)–(c). Then it abruptly, during several periods, increases up to the level approximately 5 times higher than the driver amplitude. The irregular oscillations can roughly be represented as a superposition of two modes with higher and lower amplitude. There is also seen an intermittency when for some periods of time the oscillation amplitude becomes abruptly small and then increases again. The Poincaré section in Fig. 3 (d) demonstrates the trajectory broadening and appearance of islands as is typical for stochastic regimes [1].

Further increase of the driver amplitude results in developed stochastic oscillations illustrated in Fig. 4. If the driver amplitude is equal to 1, the corresponding phase plane and Poincaré section (not shown here) are similar to ones presented in Fig. 3. If the driver amplitude, b , is equal to 5 the trajectory in the phase plane, Fig. 3 (a), is confined in the gradually broadening stripes. When the driver amplitude, b , is equal to 9 the trajectory tightly fills the confinement domain in the phase plane (see Fig. 4 (c)) showing ergodicity. The Poincaré sections in Figs.

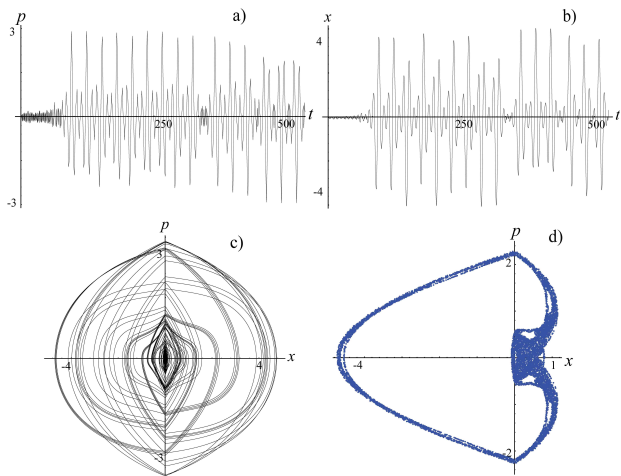


FIG. 3. Driven oscillations for the driver amplitude higher than the stochasticity threshold for $b = 0.795$, $l = 0.0125$, $p_0 = 0$, and $x_0 = 0$. a) The momentum p v.s. time. b) The coordinate x v.s. time. c) The phase plane (x, p) . d) The Poincaré section showing the particle positions in the phase plane (x, p) at the discrete time with the time step equal to the period of the driving force, 2π .

4 (b) and (d) demonstrate the formation of stability islands with the separatrices and the regions with developed stochasticity. The oscillation amplitude in Figs. 4 (a) and (b) remains finite being of the order of the driver amplitude which is typical for minimal chaos [26, 27].

Relativistic regime

In the relativistic regime the behaviour of the system (1) and (2) is governed by two dimensionless parameters, a and ε_p . In this limit, in addition to the nonlinearity due to the step like profile of the restoring force on the l.h.s. of Eq. (1), we have according to the special theory of relativity a nonlinear relationship between the particle velocity and momentum given by Eq. (2).

In the limit of small driver amplitude $a \ll \varepsilon_p$ the trajectory is confined in the vicinity of an equilibrium $x = 0$. The oscillation amplitude and frequency are of the order of $al/2\varepsilon_p$ (in dimensional units it is $eE/m_e\omega_{pe}^2$) and $(2\varepsilon_p/l)^{1/2}$, respectively. In dimensional units the oscillation frequency is equal to ω_{pe} . The condition of the displacement smallness compared to the foil width l is equivalent to the condition of low driver force frequency compared to the frequency of free oscillations. In turn it results in slow modulations of the oscillations.

Fig. 5 shows the case, when the driver amplitude being equal to $a = 0.5(\pi\varepsilon_p/2)$ for $\varepsilon_p = 15.708$ is close but lower than the resonant level. Here and below we have chosen the width $l = 0.05$, $a = 15.298$, and $\varepsilon_p = 15.708$. For $\omega_{pe}/\omega = 10$ this corresponds to the foil width of

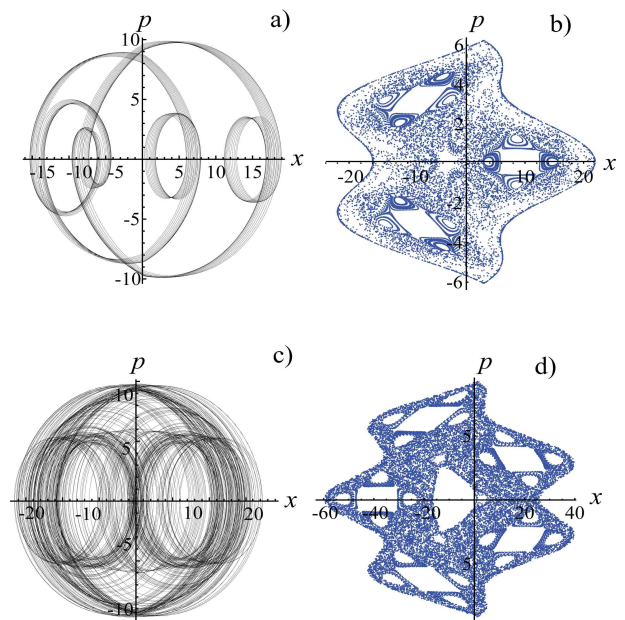


FIG. 4. Driven oscillations in near-stochastic (a,b) and stochastic (c,d) regimes for $b = 5$ and 9 , respectively, with $l = 0.00125$. a,c) The phase planes (x, p) . b,d) The Poincaré sections showing the particle positions in the phase plane (x, p) at the discrete time with the time step equal to the period of the driving force, 2π .

the order of 10 nm. As we see, the momentum amplitude $p_m \approx 0.1$ is relatively small (see Figs. 5 (a) and (b)). It remains small for a significantly long time interval. The corresponding oscillation period of the order of $4p_m/\varepsilon_p \approx 3 \times 10^{-2}$ is substantially shorter than the period of the driving force, which modulates the high frequency oscillations as seen in Fig. 5 (a). The trajectory fills the region $(-0.003 < x < 0.003, -0.15 < p < 0.15)$ of the phase plane shown in 5 (c) due to the anharmonicity of the nonlinear oscillator. The driver force also modulates the particle motion in the x direction as clearly seen in Fig. 5 (b). The Poincaré section showing the particle positions on the phase plane (x, p) at the discrete time, with the time step equal to the period of the driving force, 2π , is plotted in Fig. 5 (d). We see that the trajectory is split into two sub-loops due to the onset of the stochastic regime. This corresponds to a superposition of the regular periodic circulation and the relatively weak stochastic motion.

Under the conditions corresponding to the parameters ε_p and a above the threshold of the stochastic regime, $a = 0.62(\pi\varepsilon_p/2)$ the features of the driven nonlinear oscillators are shown in Fig. 6. As one can see, at the initial stage for the time interval $t \in [0, 60]$ the oscillation amplitude is significantly smaller than the driver amplitude (see also Fig. 7 below). Then it rises up abruptly. The maximum momentum oscillation amplitude as seen

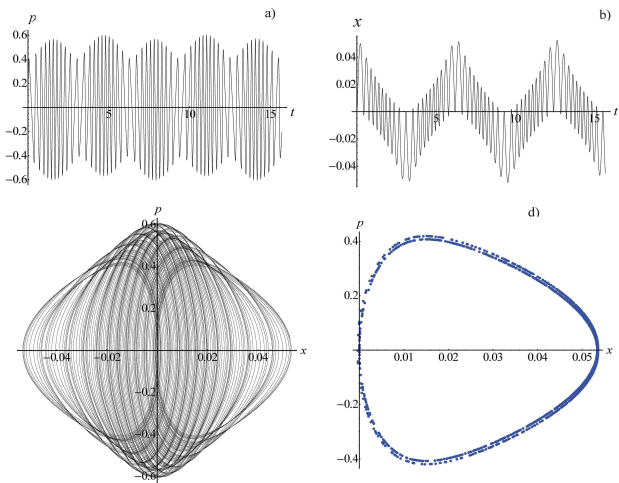


FIG. 5. Driven oscillations in nonresonant case for $\varepsilon_p = 15.708$, $a = 0.52(\pi\varepsilon_p/2) \approx 13.05$ and $l = 0.0125$. a) The momentum p v.s. time. b) The coordinate x v.s. time. c) The phase plane (x, p) for $t \in [0, 2\pi]$. d) The Poincaré section showing the particle positions in the phase plane (x, p) at discrete times, with the time step equal to the period of the driving force, 2π .

in Figs. 6 (a) and (b) reaches a level approximately 10 times higher than the driver amplitude. The time dependence of the momentum, Fig. 6 (a), and coordinate, Fig. 6 (b), demonstrate the intermittency of the irregular behaviour. This clearly demonstrates that the intervals of high amplitude, low frequency oscillations with relatively large trajectory excursion from the $x = 0$ plane randomly alternate with low amplitude, high frequency motion when the trajectory is confined in the vicinity of $x = 0$ plane. The trajectory is localized within the domain of the phase plane shown in Fig. 6 (c). The trajectory tightly fills this domain demonstrating the ergodic property of the system under consideration. The domain size increases as time grows, i. e. the particle momentum is gradually growing. In Fig. 6 (d) we plot the Poincaré section showing the particle positions in the phase plane (x, p) at discrete times, with the time step equal to the period of the driving force, 2π . It has the form of a finite thickness web (it is also known as the Arnold web [28, 29]), which is broadened due to the stochastic nature of the particle motion. The property of the particle to migrate in the phase plane along the web is typical for the minimal chaos regimes [26]. In Fig. 6 (e) the Fourier spectrum of the coordinate x is presented. Here the dependence of $\ln x_\Omega$ on the frequency Ω shows that the spectrum is continuous, which is one of the indications of the chaos regime [30].

The process of the particle energization in the initial stage is shown in Fig. 7. The intervals of regular, high frequency oscillations alternate with relatively short periods of nonadiabatic dependence of the momentum and

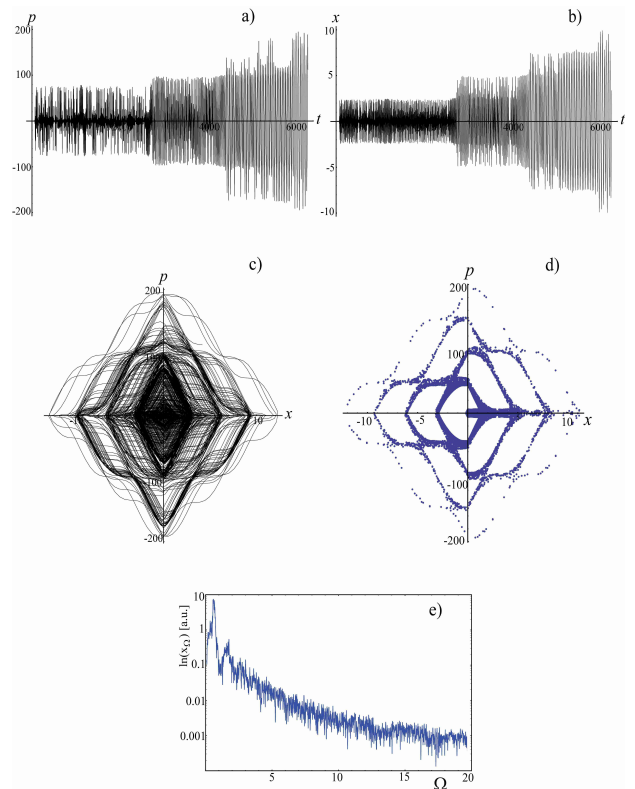


FIG. 6. Driven oscillations near the stochastic regime for $\varepsilon_p = 15.708$ and $a = 0.62(\pi\varepsilon_p/2) = 15.298$. a) The momentum p v.s. time. b) The coordinate x v.s. time. c) The phase plane (x, p) . d) The Poincaré section showing the particle positions in the phase plane (x, p) at discrete times, with the time step equal to the period of the driving force, 2π . e) Fourier spectrum of the coordinate x . The dependence of $\ln x_\Omega$ on the frequency Ω is shown.

coordinate on time. Around $t = \pi, 2\pi, 3\pi$, and so on, the trajectory is “kicked” by the driver field resulting in the momentum Fig. 7 (a) and coordinate 7 (b) amplitude increase. In the nonadiabatic phase the trajectory excursion along the x -coordinate is substantially larger than the oscillation amplitude in the adiabatic phase. Having been “kicked” several times the trajectory leaves the vicinity of the equilibrium plane $x = 0$.

To compare the phase patterns for the parameters near and above the stochasticity threshold in Fig. 8 we plot the Poincaré sections showing the particle positions in the phase plane (ϕ, p) at discrete times with the time step corresponding to the crossing of the $x = 0$ plane by the trajectory. In the case presented in Fig. 8 (a) for $\varepsilon_p = 15.708$ and $a = 0.62(\pi\varepsilon_p/2) = 15.298$ as in Fig. 6, the driven oscillator is near the threshold of the stochastic regime. The phase plane shows the overlapping relatively narrow resonances. Slightly increasing the driver amplitude, with $\varepsilon_p = 15.708$ and $a = 0.8(\pi\varepsilon_p/2) = 19.74$, we obtain the oscillations in the developed stochastic regime

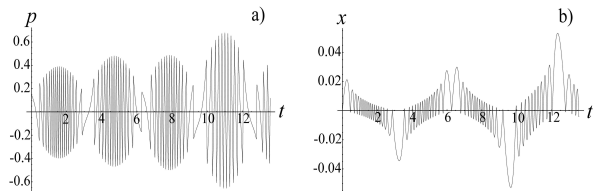


FIG. 7. Initial stage of driven oscillations in the near resonance conditions for $\varepsilon_p = 15.708$ and $a = 0.62(\pi\varepsilon_p/2) = 15.298$. at $0 < t < 4\pi$. a) The momentum p v.s. time. b) The coordinate x v.s. time.

as seen in in Fig. 8 (b). We see the overlapping of the broad stochastic layers similar to the pattern which is presented in Fig. 1 (b).

Time dependence of the average kinetic energy

In the limit of large driver amplitude, $a \gg \varepsilon_p$, the non-linear oscillations are regular. In order to determine the parameters of domains where the oscillations are stochastic and where they are regular, we analyze the time average of the kinetic energy,

$$w(t_m) = \frac{1}{(1+a^2)^{1/2} t_m} \int_0^{t_m} \left[(1+p(t)^2)^{1/2} - 1 \right] dt. \quad (48)$$

Here t_m is the averaging time. The electron kinetic energy \mathcal{E}_e is normalized by $m_e c^2 (1+a^2)^{1/2}$. In the case of particle oscillations in the driver field only, i. e. $\varepsilon_p = 0$ which is similar to the mean electron energy introduced in Ref. [5], we have

$$w_0(t_m) = \frac{2}{\pi(1+a^2)^{1/2}} \left[\frac{1}{t_m} E(t_m; -a^2) - 1 \right] \quad (49)$$

with the incomplete elliptic integral $E(x; k)$. In the limit $t_m \rightarrow \infty$ it yields for the time average of the normalized kinetic energy,

$$w_0 \approx \frac{2E(-a^2)}{\pi(1+a^2)^{1/2}}. \quad (50)$$

For $a \gg 1$ we have $w_0 \approx 2/\pi$.

In Fig. 9 we plot the parametric dependences of the time averaged normalized kinetic energy, w . Fig. 9 (a) shows the function $w(a)$ for fixed parameter ε_p . In Fig. 9 (b) we plot the function $w(\varepsilon_p)$ for fixed driver amplitude a . The dependences of the average normalized kinetic energy on the parameters a and ε_p clearly demonstrate the stochastic regions above the threshold $a = 0.62(\pi\varepsilon_p/2)$ with the width of the order of $\delta a \approx 10$ and $\delta\varepsilon_p \approx 10$. The analysis of the time dependence of the kinetic energy shows (see Fig. 10) that its growth approximately corresponds to the dependence $\propto t^\kappa$. Within a relatively

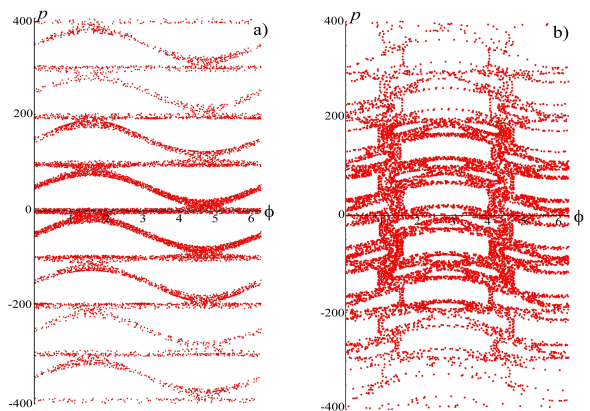


FIG. 8. The Poincaré section showing the particle positions in the phase plane (ϕ, p) at discrete times with the time step corresponding to the crossing of the $x = 0$ plane by the trajectory: a) near threshold of the stochastic regime for $\varepsilon_p = 15.708$ and $a = 0.62(\pi\varepsilon_p/2) = 15.298$; b) in the developed stochastic regime for $\varepsilon_p = 15.708$ and $a = 0.8(\pi\varepsilon_p/2) = 19.74$.

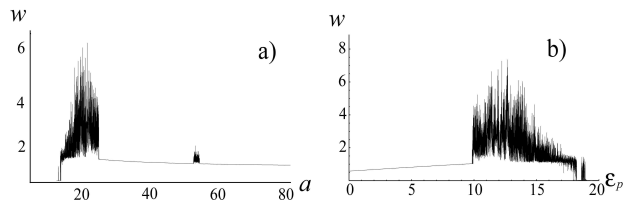


FIG. 9. Average normalized kinetic energy as a function of the driver amplitude a for the given parameter $\varepsilon_p = 15.708$, (a), and as a function of the parameter ε_p for given amplitude $a = 15.298$, (b). The averaging time is $t_m = 100 \times 2\pi$.

short time interval the index κ is close to $1/2$ as predicted by Eq. (20) although there is a significant uncertainty. Over a relatively long time interval $t \in [100, 1500]$ the averaged energy grows proportionally to $t^{1/3}$ according to Eq. (39) as seen in Fig. 10, where the time dependence of $\ln(w/t^{1/3})$ is plotted.

In Fig. 9 we can see another stochastic region in the interval $a \in [50, 60]$. In Figs. 11 and 12 we present two

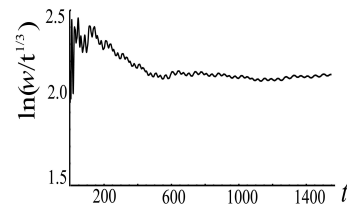


FIG. 10. Dependence on time of the average normalized kinetic energy logarithms for the driver amplitude $a = 15.708$ parameter $\varepsilon_p = 11.781$.

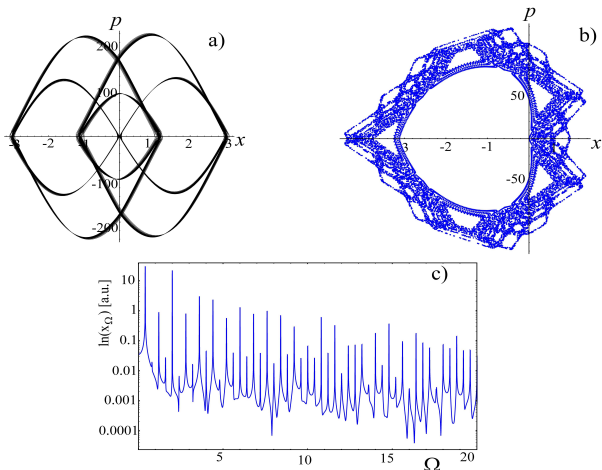


FIG. 11. Driven oscillations near stochastic regime for $\varepsilon_p = 15.708$ and $a = 9.986 \times 0.62(\pi\varepsilon_p/2) = 152.765$. a) The phase plane (x, p) . b) The Poincaré section showing the particle positions in the phase plane (x, p) at discrete times, with the time step equal to the period of the driving force, 2π . c) Fourier spectrum of the coordinate x . It is shown the dependence of $\ln x(\Omega)$ on the frequency Ω .

examples of regular dynamics described by the solutions of Eqs. (1,2) for the parameters beyond the stochastic region, i. e. $a \ll \varepsilon_p$.

In Fig. 11 we plot the phase plane (x, p) , Poincaré section and the Fourier spectrum of the coordinate x for the driver amplitude and the parameter ε_p equal to 15.708 and $a = 9.986 \times 0.62(\pi\varepsilon_p/2)$, respectively. The trajectory in the phase plane is localized in narrow width stripes. The Poincaré section shows a stochastic layer with islands around the periodic trajectory. However, the Fourier spectrum is comprised of high order harmonics, which is typical for regular nonlinear oscillations.

Slightly changing the driver amplitude to $a = 9 \times 0.62(\pi\varepsilon_p/2)$ with the same parameter ε_p as in Fig. 11 results in ergodic motion, when the trajectory completely fills the confinement domain in the phase plane (see Fig. 12 (a)). According to the Poincaré section in Fig. 12 (b) and the Fourier transform, Fig. 12 (c), consisting of high order harmonics, the nonlinear oscillations are regular with no stochastic layer.

Note that the stochastic-like regimes with developed stochastic layers seen in Figs. 11 (b) are not ergodic, i.e. the trajectory being confined within the finite size domain in the phase plane forms finite width stripes. It does not fill the domain. Contrary to this, there is an example when the regular trajectory fills the confinement domain as is seen in Fig. 12 (a).

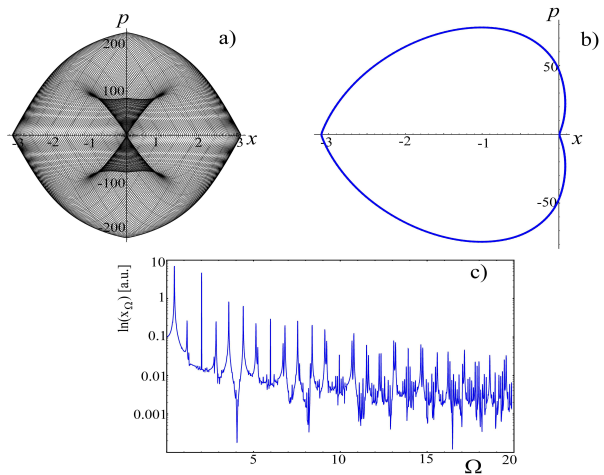


FIG. 12. Driven oscillations in regular regime for $\varepsilon_p = 15.708$ and $a = 9 \times 0.62(\pi\varepsilon_p/2) = 137.681$. a) The phase plane (x, p) . b) The Poincaré section showing the particle positions in the phase plane (x, p) at discrete times, with the time step equal to the period of the driving force, 2π . c) Fourier spectrum of the coordinate x . The dependence of $\ln x(\Omega)$ on the frequency Ω is shown.

4. CONCLUSION

In conclusion, we have demonstrated that a driven oscillator with a step-like nonlinearity can exhibit regular and chaotic oscillation regimes. The step-like nonlinearity implies a maximal value of the restoring force. The threshold of the stochastic oscillation onset corresponds to the condition of a strong driver compared with the restoring force. It can be written as a relationship between the normalized electromagnetic field amplitude and the normalized surface density: $a > \varepsilon_p$. This inequality is equivalent to the criterion of thin slab relativistic transparency [15–18]. It also determines the parameters optimal for ion acceleration by the laser light radiation pressure [17–20]. The model used above describes the anomalous electron heating due to the electron recirculation around thin foil target. We note that the electron recirculation during the ion acceleration by the light radiation pressure has been seen in theoretical work presented in Refs. [16] and [31, 32]. The electron heating can be enhanced for the tightly focused laser pulse [33] and for not perfectly aligned laser-target configurations [34].

Under the chaos conditions the oscillation amplitude grows proportionally with time to the one third power, which is an indication of the trajectory diffusion in phase space previously discussed in Ref. [8]. This result has been obtained by analyzing the Poincaré mapping, by solving the KFPE diffusion equation, and by numerical integration of an ensemble of nonlinear oscillator equations.

The obtained electron energy scaling given by Eq. (41), at the stochasticity threshold $a \approx \varepsilon_p$ in the limit $a \gg 1$ can be approximated by

$$\frac{\overline{\mathcal{E}}_e}{m_e c^2} \approx 1.11 \times \left(I \left[\frac{\text{EW}}{\text{cm}^2} \right] \right)^{1/2} \lambda [\mu\text{m}] (\tau_{las} [\text{fs}])^{1/3}, \quad (51)$$

where τ_{las} is the laser pulse duration. This scaling is favorable for achieving high energy ion beams generated under the conditions when the TNSA acceleration mechanism is realized in the laser interaction with thin foil targets. This shows substantially higher electron temperature than the scaling found in Ref. [5]. This is due to the electron recirculation around a thin foil target as has been found in PIC simulations in Refs. [35, 36] (see also Refs. [6, 7]) resulting in anomalous electron heating.

ACKNOWLEDGMENTS

This work was supported by a Scientific Research (C) No. 25420911 commissioned by MEXT and partially supported by NEXT Program of JSPS. SVB is grateful to Prof. S. I. Krasheninnikov for discussions and to Prof. F. Pegoraro for useful comments. AY appreciate fruitful discussions with Prof. S. Fujioka and H. Azechi of ILE. TZhE acknowledges the support from JSPS (Grant No. 25390135).

[1] M. Tabor, *Chaos and Integrability in Nonlinear Dynamics* (John Wiley and Sons, Inc., 1989).
 [2] J. M. T. Thompson and H. B. Stewart, *Nonlinear dynamics and chaos* (John Wiley and Sons, Inc., 2002).
 [3] F. Brunel, Phys. Rev. Lett. **59**, 52 (1987).
 [4] A. Yogo, S. V. Bulanov, M. Mori, K. Ogura, T. Zh. Esirkepov, A. S. Pirozhkov, M. Kanasaki, H. Sakaki, Y. Fukuda, P. R. Bolton, H. Nishimura, and K. Kondo, in preparation.
 [5] S. Wilks, W. L. Kruer, M. Tabak, and A. B. Langdon, Phys. Rev. Lett. **69**, 1383 (1992).
 [6] T. Taguchi, T. M. Antonsen, Jr., and H. M. Milchberg, Phys. Rev. Lett. **92**, 205003 (2004).
 [7] B. N. Breizman, A. V. Arefiev, and M. V. Fomytskyi, Phys. Plasmas **12**, 056706 (2005).
 [8] B. S. Paradkar, S. I. Krasheninnikov, and F. N. Beg, Phys. Plasmas **19**, 060703 (2012).
 [9] S. I. Krasheninnikov, Phys. Plasmas **21**, 104510 (2014).

[10] G. M. Fraiman, V. A. Mironov, and A. A. Balakin, Phys. Rev. Lett. **82**, 319 (1999).
 [11] A. Brantov, W. Rozmus, R. Sydora, C. E. Capjack, V. Y. Bychenkov, and V. T. Tikhonchuk, Phys. Plasmas **10**, 3385 (2003).
 [12] A. A. Balakin and G. M. Fraiman, JETP **103**, 370 (2006).
 [13] Z.-M. Sheng, K. Mima, Y. Sentoku, M. S. Jovanović, T. Taguchi, J. Zhang, and J. Meyer-ter-Vehn, Phys. Rev. Lett. **88**, 055004 (2002).
 [14] A. Bourdier, D. Patin, and E. Lefebvre, Laser and Particle Beams **25**, 169 (2007).
 [15] V. A. Vshivkov, N. M. Naumova, F. Pegoraro, and S. V. Bulanov, Phys. Plasmas **5**, 2727 (1998).
 [16] S. V. Bulanov, T. Zh. Esirkepov, M. Kando, S. S. Bulanov, S. G. Rykovanov, and F. Pegoraro, Phys. Plasmas **20**, 123114 (2013).
 [17] S. V. Bulanov, T. Zh. Esirkepov, M. Kando, A. S. Pirozhkov, and N. N. Rosanov, Phys. Usp. **56**, 429 (2013).
 [18] S. V. Bulanov, T. Zh. Esirkepov, M. Kando, J. Koga, K. Kondo, and G. Korn, Plasma Phys. Rep. **41**, 1 (2015).
 [19] T. Zh. Esirkepov, M. Borghesi, S. V. Bulanov, G. Mourou, and T. Tajima, Phys. Rev. Lett. **92**, 175003 (2004).
 [20] S. S. Bulanov, C. B. Schroeder, E. Esarey, and W. P. Leemans, Phys. Plasmas **19**, 093112 (2012).
 [21] E. Fermi, Phys. Rev. **75**, 1169 (1949).
 [22] E. Fermi, Astrophys. J. **119**, 1 (1954).
 [23] A. J. Lichtenberg and M. A. Lieberman, Physica D **1**, 291 (1980).
 [24] N. V. Karlov and N. A. Kirichenko, *Oscillations, Waves, Structures* (M: Fizmatgiz, 2003) (in russian).
 [25] I. S. Gradshteyn and I. M. Ryzhik, *Table of integrals. Series, and Products* (Academic, New York, 1980).
 [26] A. A. Chernikov, R. Z. Sagdeev, D. A. Usikov, M. Yu. Zakharov, and G. M. Zaslavsky, Nature **326**, 559 (1987).
 [27] F. Dyson, Phys. Uspekhi **180**, 859 (2010).
 [28] V. I. Arnold, Sov. Math. Dokl. **5**, 581 (1964).
 [29] B. V. Chirikov, Phys. Reports **52**, 263 (1979).
 [30] Y. G. Sinai, Mat. Proc. **5**, 32 (2001).
 [31] S. V. Bulanov, E. Yu. Echkina, T. Zh. Esirkepov, I. N. Inovenkov, M. Kando, F. Pegoraro, and G. Korn, Phys. Rev. Lett. **104**, 135003 (2010).
 [32] S. V. Bulanov, E. Yu. Echkina, T. Zh. Esirkepov, I. N. Inovenkov, M. Kando, F. Pegoraro, and G. Korn, Phys. Plasmas **17**, 063102 (2010).
 [33] F. Dollar, C. Zwick, A. G. R. Thomas, V. Chvykov, J. Davis, G. Kalinchenko, T. Matsuoka, C. McGuffey, G. M. Petrov, L. Willingale, V. Yanovsky, A. Maksimchuk, and K. Krushelnick Phys. Rev. Lett. **108**, 175005 (2012).
 [34] K. V. Lezhnin, F. F. Kamenets, V. S. Beskin, M. Kando, T. Zh. Esirkepov, and S. V. Bulanov, Phys. Plasmas **22**, 033112 (2015).
 [35] A. J. Kemp and L. Divol, Phys. Rev. Lett. **109**, 195005 (2012).
 [36] T. Liseykina, P. Mulser, and M. Murakami, Phys. Plasmas **22**, 033302 (2015).